3D atomic structure of supported metallic nanoparticles estimated from 2D ADF STEM images: a combination of atom-counting and a local minima search algorithm

*Ece Arslan Irmak Pei Liu Sara Bals Sandra Van Aert**

E.Arslan Irmak, P. Liu, Prof. Dr. S. Bals, Prof. Dr. S. Van Aert
EMAT and NANOlab Center of Excellence, University of Antwerp, Groenenborgerlaan 171, B-2020 Antwerp, Belgium
Email Address: sandra.vanaert@uantwerpen.be

Keywords: *supported nanoparticles, quantitative ADF STEM, 3D characterization, molecular dynamics simulations, local minima search algorithm*

Determining the three-dimensional (3D) atomic structure of nanoparticles (NPs) is critical to understand their structure-dependent properties. It is hereby important to perform such analyses under conditions relevant for the envisioned application. Here, we investigate the 3D structure of supported Au NPs at high temperature, which is of importance to understand their behavior during catalytic reactions. To overcome limitations related to conventional high-resolution electron tomography at high temperature, 3D characterization of NPs with atomic resolution has been performed by applying atom-counting using atomic resolution annular dark-field scanning transmission electron microscopy (ADF STEM) images followed by structural relaxation. However, at high temperatures, thermal displacements, which affect the ADF STEM intensities, should be taken into account. Moreover, it is very likely that the structure of a NP investigated at elevated temperature deviates from a ground state configuration, which is difficult to determine using purely computational energy minimization approaches. In this paper, we therefore propose an optimized approach using an iterative local minima search algorithm followed by molecular dynamics (MD) structural relaxation of candidate structures associated with each local minimum. In this manner, it becomes possible to investigate the 3D atomic structure of supported NPs, which may deviate from their ground state configuration.

1 Introduction

An accurate description of the morphology and the structure of metallic NPs is of great importance since these aspects determine many of their physical and chemical properties. Supported Au NPs smaller than 3-5 nm are highly reactive for a variety of important catalytic applications where the reacting molecules adsorb on the catalytically active surface. [1, 2] It has been shown that the binding energy of the reacting molecules decreases with decreasing coordination number of Au atoms at the surface. In addition, the metal-support interaction between the NP and the oxide support, often CeO_2, plays a critical role. The Au-CeO_2 interface may yield active sites leading to high catalytic activities during e.g., CO oxidation and water-gas shift reactions. [3–5] Therefore, it is essential to characterize the structure of the catalytic NPs at the atomic scale and to hereby consider the role of the support.
Among different experimental techniques, ADF STEM is a valuable technique to investigate materials at the atomic scale. ADF STEM images can be obtained with atomic resolution and the image intensity is sensitive to sample thickness and the atomic number of the elements that are present. [6–10] Nonetheless, these two-dimensional (2D) images are usually inadequate to analyze the structure-property relation of nanomaterials because they only provide a projected image of a 3D structure. Electron tomography is one of the most known and powerful methods to retrieve the 3D atomic structure of NPs. [11, 12] However, it is not always straightforward to apply conventional electron tomography since the approach requires a tilt series of many images to be acquired over a tilt range that is as large as possible. Conventional electron tomography therefore becomes very challenging when one wants to investigate very small or electron beam-sensitive NPs. Moreover, performing 3D *in situ* experiments or 3D characterization of dynamic processes is nearly impossible using conventional electron tomography since the NPs will change during the acquisition of the tilt series. Although the recently developed fast tomography approach shows great promise to accelerate the acquisition of tomographic tilt series from hours to minutes, the resolution is currently limited to the nanometer regime. [13, 14]
As an alternative method, 3D characterization of NPs with atomic resolution has been performed by combining atom-counting using statistical parameter estimation and structural relaxation. [15–19] Hereby,

a high-resolution ADF STEM image is considered as a data plane to estimate the total number of atoms in each atomic column with the highest possible precision and accuracy. [20, 21] Next, the unknown positions of the atoms are determined based on the atom-counting results by performing atomistic simulations, such as Monte Carlo (MC) or Molecular Dynamics (MD) simulations. [15, 16, 18, 19] Since the data acquisition is much faster in comparison to electron tomography, this approach enables one to study 3D dynamical changes of nanomaterials at the atomic scale during *in situ* experiments. In the past, the method has been used to investigate the structural evolution of Pt NPs under a gaseous environment, [15] to get insight into the damage mechanism of Pt NPs under the electron beam, [18] and to study 3D restructuring of Au NPs after heating to high temperature. [16]
In this study, we focus on the 3D characterization of Au NPs supported by CeO_2 at a temperature of 400 °C, at which catalytic reactions are often performed. [2, 22] In order to reliably count the number of atoms for NPs at high temperature, we show that thermal displacements of the atoms need to be taken into account since this may affect the ADF STEM intensities and hence the quantification, especially for small NPs. Moreover, we expect that supported NPs at high temperature may significantly deviate from its ground state configuration. At high temperatures, kinks and steps at the surface of the NP, acting as active sites for catalytic reactions, may appear. Also, the particle-support interaction will influence the atomic configuration at the surface of a supported NP. Hence, it is very likely that the structures of interest in this study can have a metastable state located in one of the local minima in the energy landscape, containing a huge number of local minima, each corresponding to a different atomic arrangement. [23] Purely computational energy minimization approaches, such as MC or MD simulations, may easily result in a closest local minimum where the reconstructed structure may deviate from the experimental observation. To overcome the aforementioned limitations and obtain a reliable 3D model of supported NPs at high temperatures, the energy landscape should be exhaustively explored to find the local minimum corresponding to the experimentally observed structure. [24–29] We therefore propose an iterative local minima search algorithm [30], which is followed by MD structural relaxation at the experimental temperature and by including the particle-support interaction.
In the following part, the methodology for atom-counting and 3D reconstruction is explained. Moreover, simulations of small Au NPs at high temperature have been performed to evaluate the accuracy of the atom-counting and validate the proposed 3D reconstruction methodology.

2 Results and discussion

2.1 Electron Microscopy

Au NPs on CeO_2 were prepared by a physical sputtering coating method. ADF STEM projection images of the samples were acquired using a Thermo Fisher Scientific Themis Z microscope. The electron microscope was operated at 300 keV with a 30.4 mrad probe convergence semi-angle and a beam current of 50 pA. The inner and outer detector collection angles of the ADF detector were equal to 46.1 mrad and 198.6 mrad, respectively. For the acquisition of the high-resolution projection images of the supported Au NP, a DENSsolutions *in situ* heating holder (Wildfire) was used. During the experiment, images of 1024×1024 pixels in size with a frame time of 0.629 s were recorded at 400 °C under vacuum conditions. **Figure S1**.a, shows an experimental ADF STEM image of a supported Au NP along a [110] zone axis. It can be seen that the epitaxial relationship between the support and the NP is $Au\{111\}//CeO_2\{111\}$, which is extensively observed for ceria-supported Au NPs. [31, 32]
In order to compare the experimental data with image simulations in a quantitative manner, the acquired ADF STEM images were normalized using so-called detector scan, providing an image where the intensities are proportional to the local sensitivity of the ADF detector surface. [33] **Figure S2**.a and Figure S2.b show the experimental detector scan and its radial distribution graph.

2.2 Atom-counting for NPs at high temperature

2.2.1 Accuracy of the atom-counting approach evaluated on a simulated ADF STEM image

In order to evaluate the ability to reliably count the number of atoms in NPs from experimental ADF STEM images acquired at high temperatures, atom-counting was first tested using accurate ADF STEM image simulations in which all factors affecting the image intensities were accounted for. As a test structure, a truncated octahedral Au NP (1215 atoms) was created with a size comparable to the experimentally imaged NP in Figure S1.a. Moreover, to include the NP-support interaction, a CeO_2 substrate was created according to the fluorite structure and the experimentally observed epitaxial relationship between the support and the NP. This structure was relaxed by MD simulations using the LAMMPS open source code [34] at the experimental temperature of 400 °C. To define the interaction between Au-Au atoms during the structural relaxation, the embedded atom model (EAM) [35] was used. For the interaction between the CeO_2 support and the Au NP, we used the Lennard-Jones (LJ) potential. Since the interaction between the Au NP and oxide support is sensitive to several parameters, such as the size of the NP, the orientation of the NP on the support, the epitaxial relationship between the NP and the support, steps or defects on the oxide surface as well as the experimental environment, [19, 36–38] it is important to define the particle-support interaction directly based on the experimental observation. Therefore, the average interface spacing between the NP and the CeO_2 support observed from the experimental observation (Figure S1.b), was taken as a reference to define the LJ parameters (**Figure S3**) used in MD simulations.
Next, the atomic positions of the relaxed structure (**Figure 1**.a) were used as an input for ADF STEM image simulations. Multislice calculations within the frozen phonon framework were used to accurately simulate thermal diffuse scattering in ADF STEM images. Use has been made of the MULTEM program, [39] where the simulation parameters were chosen in accordance with the experimental imaging conditions. Moreover, a temperature-dependent Debye-Waller factor (DWF) [40] and experimentally determined detector characteristics were included. [33] Next, the simulated image was convoluted with a 2D Gaussian to mimic the source size effect and Poisson noise was included corresponding to the experimental electron dose.

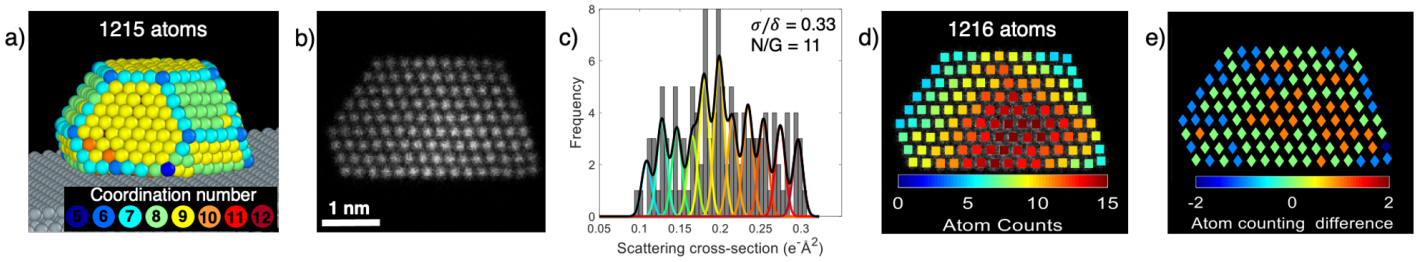

Figure 1. Summary of the methodology used to count the number of atoms demonstrated for a simulated ADF STEM image. (a) 3D model of the Au NP after structural relaxation on a CeO_2 support at 400 °C, which is used for MULTEM simulations. Au atoms are presented in different colors according to their coordination numbers. (b) Simulated ADF STEM image of the relaxed NP shown in (a). (c) Histogram of estimated SCSs together with the underlying Gaussian mixture model. The solid black curve shows the estimated Gaussian mixture model, whereas the colored curves indicate the individual normal components. (d) Number of atoms in each atomic column. (e) Difference in the total number of atoms in each projected atomic column between the reference model and the estimated number of atoms using the atom-counting method.

The simulated ADF STEM image of the Au NP imaged along the [110] zone axis, which will be used to evaluate the accuracy of the atom-counting and 3D reconstruction approach, is presented in Figure 1.b. To determine the number of atoms in each atomic column from the simulated image, the total scattered intensity corresponding to each atomic column in the NP, the so-called scattering cross-section (SCS), was extracted from the ADF STEM image using statistical parameter estimation theory as implemented in the StatSTEM open-source software. [20, 21, 41, 42] Using this approach, the images were first modeled by a superposition of Gaussian peaks located at the atomic column positions. Based on the estimated

height and width, the volume under the modeled Gaussian peak, i.e., the SCS, was determined for each projected atomic column (Figure 1.c). Next, the distribution of SCSs from all the atomic columns was decomposed into overlapping normal distributions using a so-called Gaussian mixture model analysis, [43] enabling one to determine the locations and the width of each Gaussian component (Figure 1.c). The number of Gaussian components, corresponding to the number of atoms found in the thickest atomic column, was here selected based on the known size and shape of the original structure (Figure 1.a). To determine the number of atoms in each atomic column of the simulated image, each estimated SCS was assigned to the Gaussian component with the largest probability (Figure 1.d). The estimated total number of Au atoms corresponds to 1216. The difference between the ground truth used as an input for the simulation and the estimated number of atoms for each atomic column is ±2 at maximum (Figure 1.e) but far less on average. This demonstrates the high accuracy and precision of the atom-counting methodology for NPs imaged at high temperature.

2.2.2 Counting the number of atoms from experimental images

In the previous section, a priori knowledge concerning the shape and size of the 3D original structure could be used to determine the number of components of the Gaussian mixture model. In practice, on the other hand, the number of components from experimental images is typically determined using the integrated classification likelihood (ICL) criterion. [20, 21, 42, 44] However, a correct interpretation of the ICL is affected by the overlap between the normal components and the number of columns having a specific thickness. [20] The overlap between the components can be quantified in terms of the relative width of the Gaussian components (σ/δ) where σ is the width of the normal component and δ is the distance between two neighboring components. This overlap is set by different factors including experimental detection noise, different vertical onset of columns of the same height, relaxation at the boundaries, but also by the increased thermal vibration of Au atoms at high temperature (**Figure S4**). Previous studies have shown that the number of atomic columns present in the experimental images should be sufficiently large to allow for a correct interpretation of the ICL and hence for reliable atom-counting. [20, 21, 45] If the relative width of the components (σ/δ) is of the order of 0.33, as expected from the simulation (see Figure 1.c), the required average number of atomic columns per component (N/G) should be around 90 in order to correctly count 95 % of all atomic columns, whereas it is only equal to around 11 for the small NPs investigated in this study. To overcome this problem, a time series consisting of ten frames of the same particle of interest is collected (**Figure 2**.a). By collectively analyzing all SCSs resulting from these experimental time frames, the average number of atomic columns per component (N/G) will increase to around 100, enabling a reliable interpretation of the ICL.

The estimated SCS values of the Au atomic columns obtained from ten consecutive frames are visualized in the histogram of Figure 2.b and the evaluation of the ICL criterion as a function of the number of components of the Gaussian mixture model is shown in Figure 2.c. The true number of components often corresponds to a local minimum but the presence of more than one minimum complicates the analysis. Therefore, to confirm the choice of twelve components (highlighted in red in Figure 2.c), the experimental mean SCSs (corresponding to the component locations in Figure 2.b) were compared with SCSs resulting from independent multislice simulations [21] using the MULTEM software. [39] To obtain these so-called simulated library values for increasing number of Au atoms, it is important to use the actual microscope settings, to include the contribution of thermal diffuse scattering through the frozen phonon approximation, to model the non-uniform experimentally determined detector sensitivity, and to incorporate the temperature effect by the DWF. The details regarding the multislice simulations and the effect of the detector sensitivity and temperature on the simulated library values are explained in the SI. As shown in Figure 2.d, a nearly perfect match is observed between the simulated and experimentally estimated SCSs validating the choice for twelve components where the number of atoms associated with the first component corresponds to three.

The total number of atoms in the NP and estimated number of atoms for each atomic column for the individual frames are shown in Figure 2.e and Figure 2.f, respectively. It can be seen that the estimated total number of atoms in the Au NP for the ten time frames remains almost constant over time. The

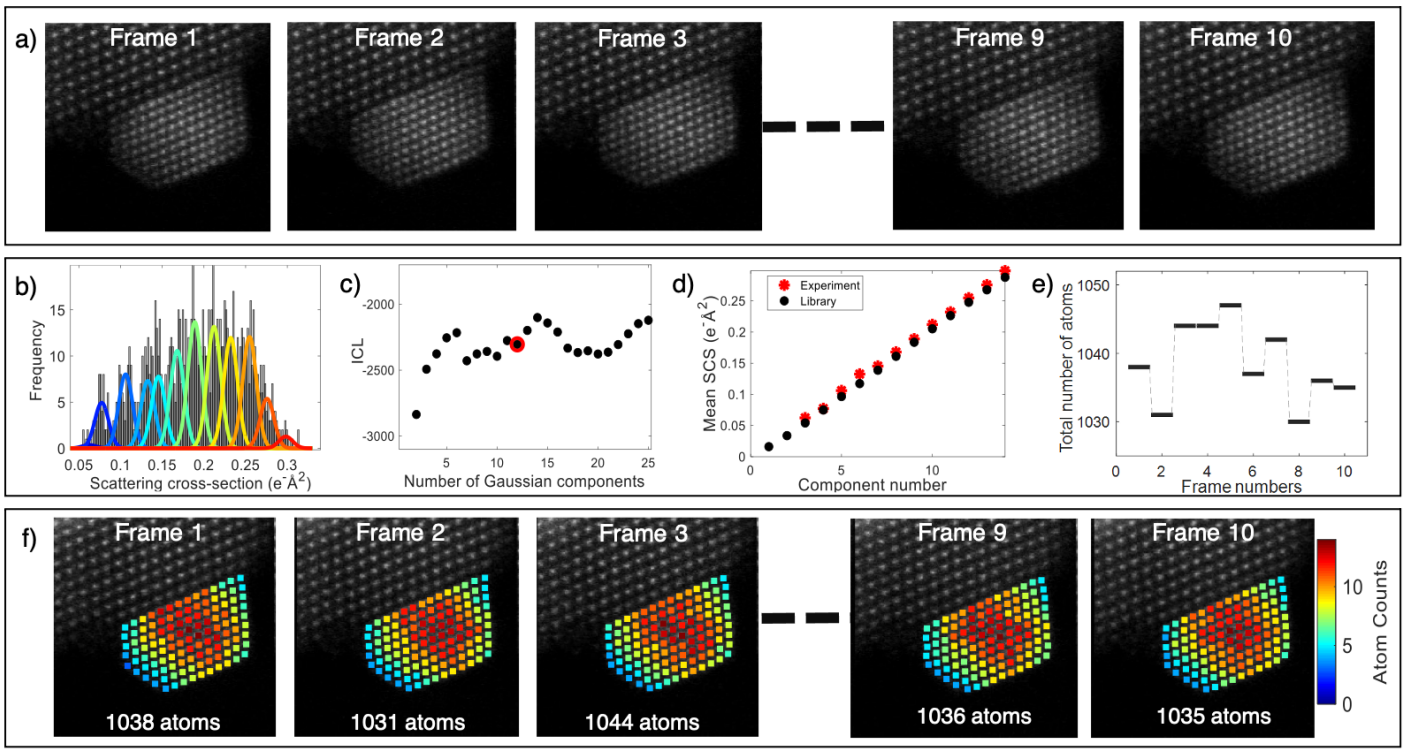

Figure 2. The ADF STEM quantification of the experimentally imaged supported Au NP at 400 °C. (a) Ten consecutive time frames. (b) Histogram of the set of SCSs of the Au columns collectively obtained from the time frames and normal components of the estimated Gaussian mixture model. (c) Evaluation of the ICL criterion. (d) Comparison of the experimentally estimated mean SCSs with the simulated library SCSs. (e) Estimated total number of atoms with respect to the frame number. (f) Atom-counting maps for all time frames.

remaining fluctuations result from the inherent experimental uncertainties and the statistical nature of the methodology. We therefore conclude that also at high temperatures and with a limited number of atomic columns, it is possible to accurately count the number of atoms for each atomic column provided that the analysis is based on a times series of images rather than on a single image and that the temperature effect is taken into account in the simulated SCSs.

2.3 3D reconstruction based on atom-counting results

2.3.1 Validation of the method based on the simulated image

Based on the estimated number of atoms for each atomic column, our final goal is to reconstruct the 3D atomic structure. The proposed method was first validated on the simulated system. The atom-counts determined in Figure 1.d were used to create a starting 3D model for the Au NP by placing the atoms symmetrically around the central plane using prior knowledge about the specimen orientation ([110]) and the crystal structure. The distance between neighboring Au atoms, parallel to the beam direction, has been fixed according to the lattice parameter (**Figure 3**.a). This provided a reliable starting input model for the next steps in our study since Au NPs on an oxide support are fairly close to being symmetrically distributed according to the thermodynamics perspective. [37]
Next, we applied an iterative local minima search algorithm to reconstruct the final 3D structure from the starting input model. The role of this step is to provide a broad sampling of the energy landscape to avoid being stuck in the closest local minimum. During each iteration step of this algorithm, a random atomic column was selected and shifted upwards or downwards in the range [-a, a], where a is the lattice parameter of the FCC Au structure. Based on the resulting change in the energy of the system, ΔE, the Boltzmann probability factor (P) was computed: [23, 46, 47]

$$P = exp(-\Delta E/k_B T) \quad (1)$$

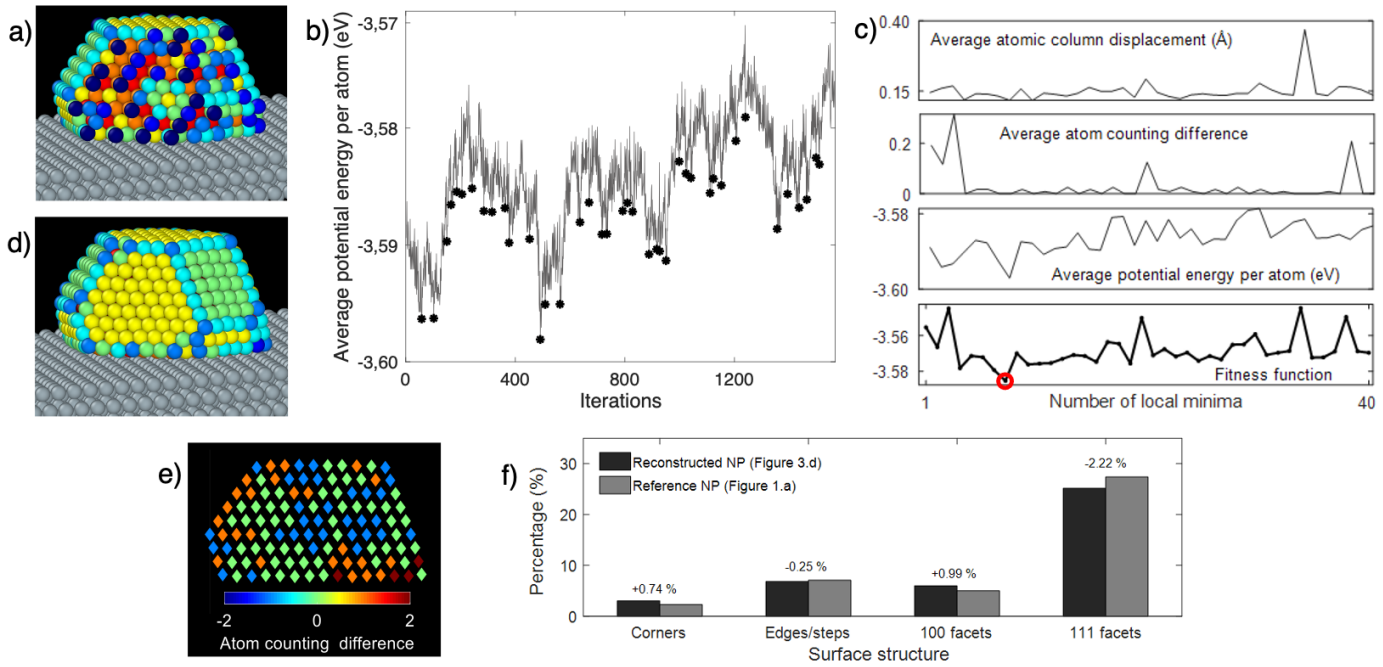

Figure 3. Main steps of the iterative local minima search algorithm demonstrated for the simulated Au NP. (a) Starting 3D model created based on the atom-counting results shown in Figure 1.d. (b) Neighborhood energy landscape obtained by the iterative local minima search algorithm. (c) The components of the defined fitness function. (d) Reconstructed final Au NP on the support. Au atoms are presented in different colors according to their coordination numbers (see Figure 1.a). (e) Difference in number of atoms in each projected atomic column between the original input and reconstructed model. (f) Comparison of the surface structure of the reconstructed NP and the original NP. The histogram is obtained from the coordination numbers of the atoms.

with k_B the Boltzmann's constant and T the temperature which was chosen as 673 K. If the value of P corresponding to the candidate structure with the displaced atoms was equal to or larger than a specified threshold, the candidate structure was accepted and used as a starting point for the next iteration. Otherwise, the previous configuration was used for the next step. This process continued for many iterations, 2000 iterations in this case, until the morphology of the candidate structure deviates from a convex shape due to the displaced atomic columns. We chose a threshold value of 0.9 to efficiently explore neighboring configurations within the energy range close to the created input model. Although a high threshold imposes a narrow energy range, it works efficiently when the algorithm already starts with a reliable input model. Moreover, it brings computational advantages since this narrow energy range enables for a neighborhood search through a relatively small number of local minima, rather than a global search with a huge number of local minima. [26] The obtained neighborhood energy landscape resulting from the iterative local minima search algorithm is illustrated as a gray line in Figure 3.b. Here, points having the lowest value in regions where at least ten previous points showed a continuously decreasing trend were selected as local minima and are indicated by black dots.

Next, each candidate structure associated with a local minimum (black dots in Figure 3.b) was relaxed by MD simulations in a canonical ensemble at 400 °C for 5 ns with Nose-Hoover thermostat to locate the low energy structures from the explored local minima. Standard energy minimization algorithms, i.e. a conjugate gradient method, are typically performed without temperature parameter, at 0K, where the surface energy anisotropy is maximal. However, at high temperatures, the surface energy anisotropy decreases, and rounded parts in the equilibrium shape or some kinks and steps at the surface which act as sources of atoms or growth sites for diffusing adatoms may appear. [37] Therefore, rather than applying a standard energy minimization [48], we here applied MD structural relaxation at a specified temperature, enabling one to investigate atomic structures that may be observed at high temperatures.

During the iterative local minima search algorithm and MD simulations, the EAM potential was used to define the interaction between the Au atoms. Moreover, the presence of the support has a strong influ-

ence on the stability of the catalytic NP and certainly affects its morphology and structure, especially under the heating environment. Therefore, the interaction between the $CeO_2\{111\}$ support and the particle, which is often neglected in many of the previous studies, [15–18] was taken into account using a LJ interaction as explained in section 2.2.
Afterwards, to select the most plausible 3D structure corresponding to the explored local minima, a fitness function (f) has been defined:

$$f = \frac{E}{atom} + \alpha\chi \tag{2}$$

$$\chi = \frac{\sum_{n=1}^{N}\sqrt{(G_{candidate}(n) - G_{ref}(n))^2}}{N} + \frac{\sum_{n=1}^{N}\sqrt{(x_{candidate}(n) - x_{ref}(n))^2 + (y_{candidate}(n) - y_{ref}(n))^2}}{N} \tag{3}$$

Equation 2 includes the average potential energy per atom ($E/atom$) and a quantitative measure of the goodness of fit of each candidate structure located in a local minimum with the reference observation (χ). A weighting parameter, α, was chosen empirically to make variations in the $E/atom$ term and the χ term of the same order of magnitude. The choice of the fitness function is based on the work of Yu et al., [49] where instead of image matching, the atom-counts and projected atomic column displacements were used to define the discrepancy between the relaxed 3D structure and the observation (Equation 3). The first term of Equation 3 determines the average difference between the number of atoms located in each projected atomic column of a candidate model and the estimated atom-counts resulting from an ADF STEM image. Here, N and G represent the number of projected atomic columns and the corresponding number of atoms in an atomic column, respectively. The second term in Equation 3 measures the average shift in the projected atomic column positions of each candidate structure compared to the atomic column positions observed in the ADF STEM image. The projected atomic column positions of the candidate structures were estimated by averaging the xy-coordinates of atoms located in the same column along the z-direction.
The evolution of the fitness function for each candidate structure and the three contributing terms are shown in Figure 3.c. The minimum value in the fitness graph (indicated with a red circle in Figure 3.c) provides the final 3D structure that has the best agreement with the reference ADF STEM image (in terms of number of atoms for each atomic column and projected atomic column position) among all relaxed candidate structures associated with different local minima. The retrieved structure (Figure 3.d) is mainly composed of {100} (green atoms) and {111} (yellow atoms) facets which are separated by edges (light blue atoms) and corners (dark blue atoms). Since we have the exact 3D model (Figure 1.a) of the reference ADF STEM image, a one-to-one comparison has been made to quantitatively verify the proposed methodology. For this purpose, the difference in the number of atoms in each projected atomic column between the reconstructed NP and original input model used for MULTEM simulations was determined (Figure 3.e). It can be seen that the total number of atoms in each atomic column differs maximum ±2 atoms but far less on average. This discrepancy results from the limited precision of the statistics-based atom-counting method and the atom movement between the atomic columns during MD structural relaxations. Furthermore, a surface structure analysis was performed by determining the coordination number of all surface atoms. The comparison between the surface structures of the reconstructed NP and the original 3D model has been shown in Figure 3.f. According to the results, it can be concluded that the surface structure of the reconstructed Au NP has been identified with an accuracy of more than 95 % where the maximum difference of 2.22 % was observed in the percentage of {111} facets as indicated in Figure 3.f.

2.3.2 Experimental results

The iterative local minima search algorithm was then applied to reconstruct the 3D structure of the experimentally investigated NP (Figure 2). The reconstructed 3D atomic structures of the supported NP from ten consecutive time frames and their surface structures are illustrated in **Figure 4**.a and Figure

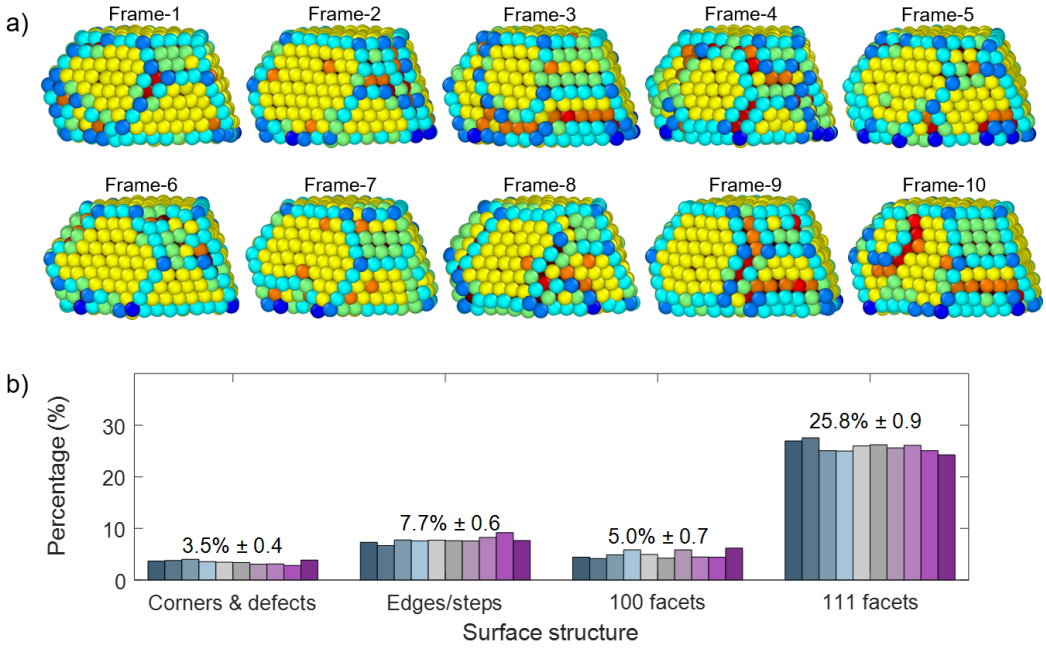

Figure 4. 3D characterization of the experimentally observed Au NP on CeO_2 retrieved from 10 consecutive time frames. (a) 3D structures where atoms are presented in different colors according to their coordination numbers. (b) Surface structure of the reconstructed NPs. The histogram is obtained from the coordination number of the atoms.

4.b, respectively. According to the percentage of the average coordination number from each reconstructed NP and the standard deviation from the mean value, indicated in Figure 4.b, the surface structure of the NP was reconstructed with high precision. The standard deviation mainly comes from atom diffusion under the electron beam, limited precision of the atom-counting method and the optimization algorithm. Around 3.5 % of the atoms are located at the corners, 7.7 % of the atoms are on edges or surface steps, 5.0 % and 25.8 % of the atoms are located on {100} and {111} surface facets, respectively.

2.4 Discussion

We tested the performance of the proposed methodology by comparing it to the outcome determined using previously applied approaches in the literature where 3D atom-counting results were combined with a MC approach or MD simulations. [15, 16, 18] For this purpose, energy minimization by a MC approach and full structural relaxation by MD simulations were performed on the same starting 3D model shown in Figure 3.a. Then the outcome of each method was compared with the original 3D structure (Figure 1.a and **Figure 5**.a).

When using the MC approach, movement of atoms between the atomic columns was not allowed and only the z-positions of the atomic columns moved up and downwards for each iteration while keeping the number of atoms in each atomic column fixed. The new configuration is accepted only if the potential energy decreases. This process was repeated until the potential energy of the system remains unchanged. The final 3D model obtained from this methodology is shown in Figure 5.b. Since the atoms were not permitted to move between the atomic columns during the MC approach, the final structure was likely affected by the limited precision of atom-counting. [16] The counting imprecision, with an error of ± 2 as explained in Section 2.2, and the restriction in the atomic movement between columns resulted in more roughness at the surface of the 3D reconstructed NP compared to the original model in Figure 5.a. In the second approach, full structural relaxation at 400 °C was performed by MD simulations for 5 ns where the NP-support interaction is ignored. According to the 3D model shown in Figure 5.c, MD simulations ended up with relatively large structural deviations from the original model due to the large atomic movement between the columns during the structural relaxation at high temperature. However, when using the method proposed in this work (Figure 5.d), there has been visually a very good agreement with the original structure.

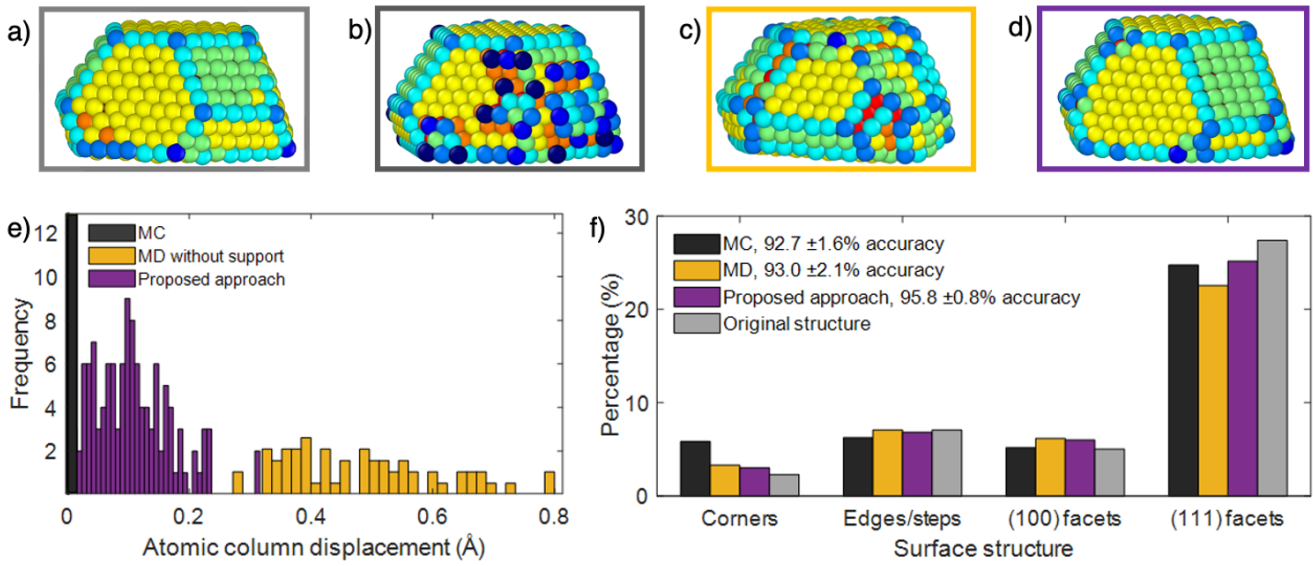

Figure 5. Comparison of different approaches. (a) Original structure. (b-d) The final structures obtained from MC approach, MD simulations and local minima search algorithm. (e) Projected atomic column displacement compared to the target structure. (f) Comparison of the surface structure of the reconstructed nanoparticles and the original nanoparticle. The histogram is obtained from the coordination number of the atoms.

Moreover, a quantitative comparison has been performed between the different approaches. Figure 5.e shows the difference in the projected atomic column positions of each reconstructed NP with respect to the atomic column positions of the original structure. Here, larger atomic column displacements indicate a large deviation of the projected structure from the observed structure in the reference ADF STEM image. Since atomic movement was not allowed during energy minimization by the MC approach, no atomic column displacements were observed (black color in Figure 5.e) so that the reconstructed particle had the same projected shape as observed in the ADF STEM image. However, more roughness was observed at the surface due to the restriction in the atomic movement between the columns. This is clear from Figure 5.f where the surface structure is determined from a coordination number analysis. Indeed, a larger percentage in the low-coordinated corner atoms is observed for the particle reconstructed using the MC approach. As it has already been observed in Figure 5.c, the discrepancy between the NP shape retrieved from MD structural relaxations and the original structure can also be seen from the large atomic column displacements (yellow color in Figure 5.e). However, the proposed local minima search algorithm (Figure 5.d) successfully reproduced the target structure both in terms of the projected atomic column positions and the atomic configuration at the surface.

The original test structure (Figure 1.a), a truncated octahedron, is a thermodynamically stable structure for Au NPs with clear surface facets. On the other hand, it is known that metastable structures have rough surfaces containing some defects. Therefore, our approach was also tested on a metastable structure. Details for the simulations of the metastable structure are explained in the SI. According to the results shown in **Figure S5**, our approach provides a significant advantage for the 3D characterization of the metastable structures compared to MC and MD methods.

It should be noted that our approach shows similarities with the basin-hopping algorithm. [23, 24, 30] However, due to the system-specific needs, it was necessary to adapt the algorithm for our system. In the basin-hopping algorithm, a standard energy minimization approach is performed at each step without temperature parameter, at 0K. Since the structure of nanoparticles depends on temperature, we here preferred to apply MD structural relaxation at a specified temperature rather than an energy minimization approach. Since performing structural relaxations at each step by including the particle-support interaction and the effect of temperature is computationally expensive, we employed a computationally more efficient model without sacrificing accuracy. For this purpose, we first obtained the neighborhood energy landscape. Afterward, to use computer resources efficiently, we eliminated the local maxima and

unstable points of the energy landscape and applied molecular dynamics simulations only for the structures located in regions of interest of the energy landscape where at least ten previous points showed a continuously decreasing trend.
Overall, with the combination of atom-counting and an iterative local minima search algorithm, where both the temperature effect and particle-support interaction were taken into account, we successfully reconstructed the 3D structure of the simulated and experimentally imaged supported NPs with high accuracy and precision. Since the proposed method does not only rely on energy minimization, it outperforms the previously applied approaches, where 3D atom-counting results were combined with a MC approach or MD simulations. [15, 16, 18] Figure 5 and Figure S5 show that the MC approach may lead to wrong interpretations for the surface-catalytic property relation, while the full MD structural relaxation can easily end up with a different structure from the originally imaged NP. However, the proposed approach in this study enables us to overcome those limitations. Due to its ability to search the local energy landscape and to find the local minimum that corresponds to the imaged NP, the original target structures observed from ADF STEM images can be successfully estimated both in terms of atomic column positions and atomic configuration at the surface. Therefore, the proposed methodology provides a powerful approach to retrieve 3D atomic-scale information of both stable and metastable structures under a catalytic environment, i.e., at high temperature.

3 Conclusion

In conclusion, we have demonstrated how a local minima search algorithm based on atom-counts resulting from ADF STEM images can be used to successfully reconstruct the 3D atomic structure of supported gold NPs even at high temperatures. This approach is initiated with a reliable starting configuration based on the atom-counting results where the atoms are positioned symmetrically along the beam direction. The proposed method, taking both the effect of experimental temperature and particle-support interaction into account, explores different local minima in the energy landscape while quantitatively validating the reconstructed structure with the observations from ADF STEM images. In this manner, atomic-scale information of supported NPs observed at high temperatures are accurately reconstructed from 2D ADF STEM images acquired along a single viewing direction. We have tested the accuracy of this method on a simulated Au NP lying on a support by considering all experimental parameters that may affect the image intensities and quantification. According to the results, the proposed method predicts the 3D atomic structure of a simulated Au NP on CeO_2 support with high accuracy and outperforms the previously reported approaches. This method, therefore, enables an accurate refinement of experimentally observed 3D atomic structures providing critical information to understand the structure-property relationship from limited data.

Supporting Information
Supporting Information is available from the Wiley Online Library or from the author.

Acknowledgements
This work was supported by the European Research Council (Grant 815128 REALNANO to SB, Grant 770887 PICOMETRICS to SVA, Grant 823717 ESTEEM3). The authors acknowledge financial support from the Research Foundation Flanders (FWO, Belgium) through project funding (G.0267.18N, G.0502.18N, G.0346.21N).

References

[1] C. Zhang, A. Michaelides, S. J. Jenkins, *Phys. Chem. Chem. Phys.* **2011**, *13* 22.

[2] B. Hvolbæk, T. V. Janssens, B. S. Clausen, H. Falsig, C. H. Christensen, J. K. Nørskov, *Nano Today* **2007**, *2*, 4 14.

[3] M. Ziemba, M. V. Ganduglia-Pirovano, C. Hess, *Faraday Discuss* **2021**, *229* 232.

[4] M. A. Centeno, T. Ramírez Reina, S. Ivanova, O. H. Laguna, J. A. Odriozola, *Catalysts* **2016**, *6*, 10.

[5] Q. Fu, *Science* **2003**, *301*, 5635 935.

[6] L. Jones, *IOP Conference Series: Materials Science and Engineering* **2016**, *109* 012008.

[7] O. L. Krivanek, M. F. Chisholm, V. Nicolosi, T. J. Pennycook, G. J. Corbin, N. Dellby, M. F. Murfitt, C. S. Own, Z. S. Szilagyi, M. P. Oxley, S. T. Pantelides, S. J. Pennycook, *Nature* **2010**, *464*, 7288 571.

[8] J. M. LeBeau, S. D. Findlay, L. J. Allen, S. Stemmer, *Nano Letters* **2010**, *10*, 11 4405.

[9] A. Rosenauer, T. Mehrtens, K. Müller, K. Gries, M. Schowalter, P. V. Satyam, S. Bley, C. Tessarek, D. Hommel, K. Sebald, M. Seyfried, J. Gutowski, A. Avramescu, K. Engl, S. Lutgen, *Ultramicroscopy* **2011**, *111*, 8 1316.

[10] E. J. Kirkland, M. G. Thomas, *Ultramicroscopy* **1996**, *62*, 1-2 79.

[11] S. Bals, B. Goris, L. M. Liz-Marzán, G. VanTendeloo, *Angewandte Chemie International Edition* **2014**, *53*, 40 10600.

[12] G. Möbus, B. J. Inkson, *Materials Today* **2007**, *10*, 12 18.

[13] H. Vanrompay, A. Skorikov, E. Bladt, A. Béché, B. Freitag, J. Verbeeck, S. Bals, *Ultramicroscopy* **2021**, *221* 113191.

[14] S. Koneti, L. Roiban, F. Dalmas, C. Langlois, A.-S. Gay, A. Cabiac, T. Grenier, H. Banjak, V. Maxim, T. Epicier, *Materials Characterization* **2019**, *151* 480.

[15] T. Altantzis, I. Lobato, A. De Backer, A. Béché, Y. Zhang, S. Basak, M. Porcu, Q. Xu, A. Sánchez-Iglesias, L. M. Liz-Marzán, G. Van Tendeloo, S. Van Aert, S. Bals, *Nano Letters* **2019**, *19*, 1 477.

[16] A. De Backer, L. Jones, I. Lobato, T. Altantzis, B. Goris, P. D. Nellist, S. Bals, S. Van Aert, *Nanoscale* **2017**, *9* 8791.

[17] S. Bals, S. Van Aert, C. P. Romero, K. Lauwaet, M. J. Van Bael, B. Schoeters, B. Partoens, E. Yücelen, P. Lievens, G. Van Tendeloo, *Nature Communications* **2012**, *3*, 1 897.

[18] L. Jones, K. E. MacArthur, V. T. Fauske, A. T. J. van Helvoort, P. D. Nellist, *Nano Letters* **2014**, *14*, 11 6336.

[19] P. Liu, E. Arslan Irmak, A. De Backer, A. De wael, I. Lobato, A. Béché, S. Van Aert, S. Bals, *Nanoscale* **2021**, *13* 1770.

[20] A. De Backer, G. Martinez, A. Rosenauer, S. Van Aert, *Ultramicroscopy* **2013**, *134* 23—33.

[21] S. Van Aert, A. De Backer, G. T. Martinez, B. Goris, S. Bals, G. Van Tendeloo, A. Rosenauer, *Phys. Rev. B* **2013**, *87* 064107.

[22] Q. Fu, H. Saltsburg, M. Flytzani-Stephanopoulos, *Science* **2003**, *301*, 5635 935.

[23] R. Ferrando, *Journal of Nanoparticle Research* **2018**, *20*, 7 179.

[24] S. Yang, G. M. Day, *Journal of Chemical Theory and Computation* **2021**, *17*, 3 1988.

[25] S. M. Woodley, R. Catlow, *Nature Materials* **2008**, *7*, 12 937.

[26] A. R. Oganov, C. W. Glass, *The Journal of Chemical Physics* **2006**, *124*, 24 244704.

[27] Q. Zhu, A. R. Oganov, C. W. Glass, H. T. Stokes, *Acta Crystallographica Section B* **2012**, *68*, 3 215.

[28] F. Curtis, X. Li, T. Rose, Á. Vázquez-Mayagoitia, S. Bhattacharya, L. M. Ghiringhelli, N. Marom, *Journal of Chemical Theory and Computation* **2018**, *14*, 4 2246.

[29] V. E. Bazterra, M. B. Ferraro, J. C. Facelli, *The Journal of Chemical Physics* **2002**, *116*, 14 5992.

[30] G. Rossi, R. Ferrando, *Journal of Physics: Condensed Matter* **2009**, *21*, 8 084208.

[31] T. Uchiyama, H. Yoshida, Y. Kuwauchi, S. Ichikawa, S. Shimada, M. Haruta, S. Takeda, *Angewandte Chemie International Edition* **2011**, *50*, 43 10157.

[32] P. Liu, T. Wu, J. Madsen, J. Schiøtz, J. B. Wagner, T. W. Hansen, *Nanoscale* **2019**, *11* 11885.

[33] F. F. Krause, M. Schowalter, T. Grieb, K. Müller-Caspary, T. Mehrtens, A. Rosenauer, *Ultramicroscopy* **2016**, *161* 146.

[34] Lammps molecular dynamics simulator, `https://www.lammps.org/index.html`.

[35] G. Grochola, S. P. Russo, I. K. Snook, *The Journal of Chemical Physics* **2005**, *123*, 20 204719.

[36] Y. Han, R. Ferrando, Z. Y. Li, *The Journal of Physical Chemistry Letters* **2014**, *5*, 1 131.

[37] C. R. Henry, *Progress in Surface Science* **2005**, *80*, 3 92.

[38] Y. Lin, Z. Wu, J. Wen, K. Ding, X. Yang, K. R. Poeppelmeier, L. D. Marks, *Nano Letters* **2015**, *15*, 8 5375.

[39] I. Lobato, S. Van Aert, J. Verbeeck, *Ultramicroscopy* **2016**, *168* 17.

[40] H. X. Gao, L.-M. Peng, *Acta Crystallographica Section A Foundations of Crystallography* **1999**, *55*, 5 926.

[41] A. De Backer, K. van den Bos, W. Van den Broek, J. Sijbers, S. Van Aert, *Ultramicroscopy* **2016**, *171* 104.

[42] S. Van Aert, K. J. Batenburg, M. D. Rossell, R. Erni, G. Van Tendeloo, *Nature* **2011**, *470*, 7334 374.

[43] G. J. McLachlan, S. X. Lee, S. I. Rathnayake, *Annual Review of Statistics and Its Application* **2019**, *6*, 1 355.

[44] C. Biernacki, G. Celeux, G. Govaert, *IEEE Transactions on Pattern Analysis and Machine Intelligence - PAMI* **1997**.

[45] A. D. wael, A. de Backer, L. Jones, P. Nellist, S. V. Aert, *Ultramicroscopy* **2017**, *177* 69.

[46] S. Kirkpatrick, C. D. Gelatt, M. P. Vecchi, *Science* **1983**, *220*, 4598 671.

[47] N. Metropolis, A. W. Rosenbluth, M. N. Rosenbluth, A. H. Teller, E. Teller, *The Journal of Chemical Physics* **1953**, *21*, 6 1087.

[48] D. J. Wales, J. P. K. Doye, *The Journal of Physical Chemistry A* **1997**, *101*, 28 5111–5116.

[49] M. Yu, A. B. Yankovich, A. Kaczmarowski, D. Morgan, P. M. Voyles, *ACS Nano* **2016**, *10*, 4 4031.

Table of Contents

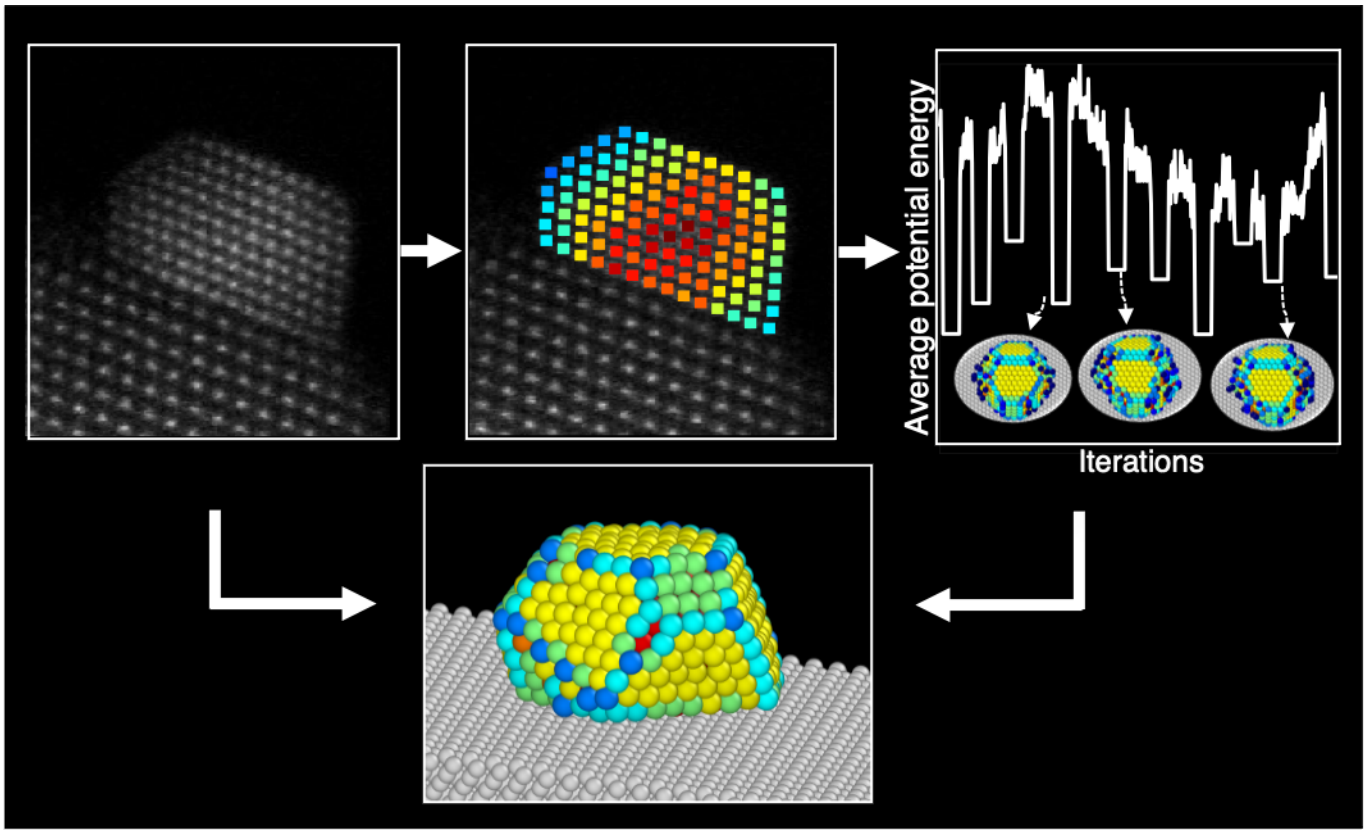

The combination of atom counting based on annular dark-field scanning transmission electron microscopy images and an iterative local minima search algorithm followed by molecular dynamics structural relaxation accurately reveals the three-dimensional atomic structure of supported metallic nanoparticles. The proposed approach provides crucial information to understand the structure-property relationship of supported metallic nanoparticles even at high temperatures.